
Neural Topographic Factor Analysis for fMRI Data

Eli Z. Sennesh^{*12} Zulqarnain Khan^{*3} Yiyu Wang² Amirreza Farnoosh³ Sarah Ostadabbas³ Jennifer Dy³
Ajay B. Satpute² J. Benjamin Hutchinson⁴ Jan-Willem van de Meent¹

Abstract

Neuroimaging studies produce gigabytes of spatio-temporal data for a small number of participants and stimuli. Recent work increasingly suggests that the common practice of averaging across participants and stimuli leaves out systematic and meaningful information. We propose Neural Topographic Factor Analysis (NTFA), a deep generative model that parameterizes factors in terms of embeddings for participants and stimuli. We evaluate NTFA on data from an in-house pilot experiment, as well as two publicly available datasets. We demonstrate that inferring representations for participants and stimuli improves predictive generalization to unseen data when compared to existing methods. NTFA infers meaningful embeddings without supervision, circumventing the assumptions that experimenters defined stimulus conditions and that subject variance is error. We also demonstrate that the inferred latent factor representations are useful for downstream tasks such as multivoxel pattern analysis and functional connectivity.

1. Introduction

Analyzing neuroimaging studies is both a large data problem and a small data problem. A single scanning run typically involves hundreds of full-brain scans that each consist of tens of thousands of spatial locations (known as voxels). At the same time, neuroimaging studies tend to have limited statistical power; a typical study considers a cohort of 20-50 participants undergoing tens of stimuli from ten (or fewer) stimulus categories. Developing methods that scale to gi-

gabytes of data, yet represent uncertainty about individual participants and stimuli, remains an open problem.

In this paper, we develop Neural Topographic Factor Analysis (NTFA)¹, a family of generative models for analysis of spatio-temporal fMRI data that explicitly represents variation among participants and stimuli. NTFA extends Topographic Factor Analysis (TFA), an established method (Manning et al., 2014b), by incorporating a deep generative prior. This prior defines a distribution over embeddings (i.e. vectors of features) for each participant and stimulus, along with a conditional distribution over spatial and temporal factors that is parameterized by a low-capacity neural network. The result is a structured deep probabilistic model that can characterize variation and interaction among participants and stimuli.

Our experiments compare NTFA to hierarchical topographic factor analysis (HTFA) (Manning et al., 2014a; 2018), an extension of TFA that employs a shared Gaussian prior over factor parameters. We evaluate NTFA on four datasets:

- As a basic validation of our model, we show that in a synthetic dataset simulated from clearly distinguishable clusters of participants and stimuli, inference recovers the underlying cluster structure.
- We present results for a pilot study, conducted by the authors, which investigates whether threat-relevant stimuli from different categories induce the same or different patterns of neural response. NTFA learns stimulus embeddings without supervision that group according to stimulus categories, albeit with some overlap.
- We consider two publicly available datasets. In the first, participants with major depressive disorder and controls listened to emotionally valenced audio stimuli and music (Lepping et al., 2016). In the second, participants viewed images of faces, cats, five categories of man-made objects, and scrambled pictures (Haxby et al., 2001). In both cases NTFA is able to infer embedding structure that is consistent with previously reported findings.

This work makes both neuroscientific and machine learning contributions. From a machine learning perspective, NTFA is a novel deep probabilistic extension of factor analysis

^{*}Equal contribution ¹Khoury College of Computer Science, Northeastern University, Boston, Massachusetts, USA ²Department of Psychology, Northeastern University, Boston, Massachusetts, USA ³Department of Electrical and Computer Engineering, Northeastern University, Boston, Massachusetts, USA ⁴Department of Psychology, University of Oregon, Eugene, Oregon, USA. Correspondence to: Eli Z. Sennesh <esennesh@ccis.neu.edu>, Zulqarnain Khan <khan.zu@ece.neu.edu>.

¹Source code submitted with paper and available upon request.

methods. The inferred embeddings capture similarities in the neural response across participants and stimuli. This improves prediction on held-out data for unseen participant-stimulus pairs, while requiring fewer trainable parameters.

From a neuroscientific perspective, the generative model in NTFA contributes to our ability to perform whole-brain analyses that characterize individual variation. Psychological states (e.g. emotions and memories) involve widely distributed patterns of activation throughout the brain (Haxby et al., 2001). Existing methods for whole-brain multivoxel pattern analysis (MVPA) often use the stimulus and participant labels for feature selection and classification (Pereira et al., 2009). In affective neuroscience, for example, an ANOVA is often performed on each voxel in the brain to identify the brain voxels that maximally differentiate between labels (e.g. “anger”, “fear”, “happiness”). Their activations serve as features for classification, once again with the same labels. In contrast, inference in an unsupervised generative model such as HTFA or NTFA does not use experimenter-defined labels. Latent factors from NTFA and HTFA thus enable whole-brain MVPA with no supervised feature-selection step. These latent factors can also be used to create data-driven functional connectomes, as opposed to using standard brain parcellations.

We summarize the contributions of this paper as follows:

- We develop NTFA (Section 3), a new generative model for fMRI data that infers shared embeddings for participants and stimuli across experiment trials.
- We show that NTFA improves generalization to unseen participant-stimulus pairs (Section 4) in terms of log-predictive probability of unseen data relative to HTFA, while employing fewer trainable parameters (Section 5).
- We demonstrate that stimulus embeddings, learned without supervision, correlate with experimental design variables (Section 5). To our knowledge, NTFA is the first model able to characterize stimuli this way.
- We demonstrate that latent factors learned by NTFA can be used in downstream neuroimaging tasks, such as MVPA and functional connectivity. (Section 5.3).

Figure 1 outlines our proposed approach. Section 2 covers related work in factor analysis for neuroimaging data, primarily the TFA and HTFA methods on which we build. Section 3 develops the NTFA model. Section 4 discusses our architectural details, preprocessing steps, and experiments. Section 5 discusses and evaluates experimental results.

2. Background

Factor analysis methods are widely used to reduce the dimensionality of neuroimaging data. These methods decompose the fMRI signal for a trial $Y \in \mathbb{R}^{T \times V}$ with T time points and V voxels into a product $Y \simeq W \cdot F$ between a

lower-rank matrix of weights $W \in \mathbb{R}^{T \times K}$ and a lower-rank matrix of factors $F \in \mathbb{R}^{K \times V}$. The dimension $K \ll V$ is chosen to balance the degree of dimensionality reduction and the reconstruction accuracy. Standard methods that have been applied to fMRI data include Principal Component Analysis (Abdi & Williams, 2010) and Independent Component Analysis (Hyvärinen et al., 2001). There are also methods that have been specifically developed for fMRI analysis, including hyper-alignment (HA) (Haxby et al., 2011), topographic latent source analysis (TLSA) (Gershman et al., 2011; 2014), topographic factor analysis (TFA) (Manning et al., 2014b), and hierarchical topographic factor analysis (HTFA) (Manning et al., 2014a; 2018). TLSA separates out a loading matrix for experimental design covariates from the weights and factors, but has otherwise the same generative model as HTFA. These models define spatially smooth factors via radial basis functions, and represent the state of the art in decomposing neuroimaging data.

In this paper, we extend TFA with a deep generative model that can consider nonlinear transformations of the two dominant covariates in neuroimaging, the participant and the stimulus. This allows us to achieve better reconstruction performance than HTFA with fewer parameters.

2.1. The TFA and HTFA generative models

We consider the task of modeling data that comprises N trials (i.e. continuous recordings), each of which contain T time points for voxels at V spatial positions. TFA approximates each trial separately $Y_n \simeq W_n F_n$ as a product between a matrix of K time-varying weights $W_n \in \mathbb{R}^{T \times K}$ and a matrix $F_n \in \mathbb{R}^{K \times V}$ of K spatially-varying factors. To do so, TFA assumes that the data is noisily sampled from the inner product between the weights and factors matrices

$$Y_n \sim \mathcal{N}(W_n \cdot F_n, \sigma^Y). \quad (1)$$

The prior $p(W_n, F_n) = p(W_n) p(F_n)$ factorizes over W_n and F_n . The prior over weights $p(W_n)$ is a hierarchical Gaussian with hyperparameters $\mu_{n,k}^W$ and $\sigma_{n,k}^W$,

$$W_{n,t,k} \sim \mathcal{N}(\mu_{n,k}^W, \sigma_{n,k}^W), \quad \mu_{n,k}^W \sim p(\mu^W), \quad \sigma_{n,k}^W \sim p(\sigma^W),$$

To define a prior over factors $p(F_n)$, TFA employs a kernel function that ensures spatial smoothness of factor values $F_{n,k,v}$ at nearby voxel positions $x_v^G \in \mathbb{R}^3$. This kernel function κ is normally a radial basis function (RBF), which models each factor $k \in \{1 \dots K\}$ as a Gaussian with center at a spatial location $x_{n,k}^F \in \mathbb{R}^3$, whose width is determined by the kernel hyper-parameters $\rho_{n,k}^F$,

$$F_{n,k,v} = \kappa(x_v^G, x_{n,k}^F; \rho_{n,k}^F), \quad (2)$$

with priors over both positions and widths,

$$x_{n,k}^F \sim p(x^F), \quad \rho_{n,k}^F \sim p(\rho^F). \quad (3)$$

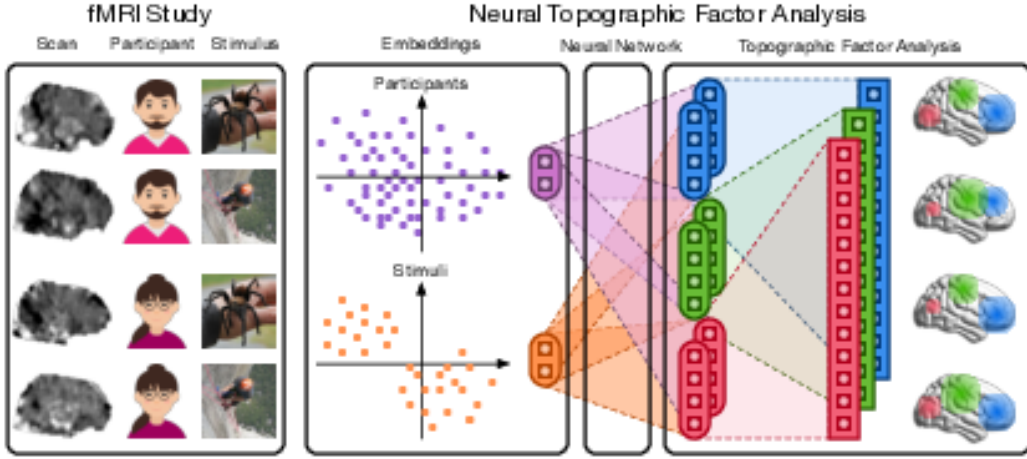


Figure 1. Overview of Neural Topographic Factor Analysis (NTFA): We extend topographic factor analysis (TFA) (Manning et al., 2014b;a) to decompose the fMRI signal into Gaussian factors (shown in red, green and blue in the figure) that correspond to spatially and temporally related brain activity across individuals. A typical fMRI study consists of multiple trials of participants undergoing scans while experiencing different stimuli (or performing different tasks). In our generative model we represent these participants (purple) and stimuli (orange) with embedding vectors. A decoder network then predicts the location, size, and mean response of the Gaussian factors.

Interpreting factor analysis generatively enables us to incorporate additional assumptions to capture similarities across a set of related trials. HTFA (Manning et al., 2014a; 2018), introduces variables \bar{x}_k^F and $\bar{\rho}_k^F$ representing each factor’s mean positions and widths across trials,

$$x_{n,k}^F \sim p(x_{n,k}^F | \bar{x}_k^F), \quad \bar{x}_k^F \sim p(\bar{x}^F), \quad (4)$$

$$\rho_{n,k}^F \sim p(\rho_{n,k}^F | \bar{\rho}_k^F), \quad \bar{\rho}_k^F \sim p(\bar{\rho}^F). \quad (5)$$

HTFA assumes that brain layouts and activations across trials vary randomly relative to a shared prior, also known as a template. This prior can represent multimodal responses to an extent, in the sense that factor positions and widths for trials are allowed to vary relative to a shared mean. However, the Gaussian hyperprior in HTFA assumes a unimodal distribution for average neural responses across trials.

TFA combines the likelihood $p(Y_n | W_n, F_n)$ with the prior $p(W_n, F_n)$ to define a probabilistic model $p(Y_n, W_n, F_n)$. Black-box methods are then used to approximate the posterior $p(W_n, F_n | Y_n)$ with a mean-field variational distribution $q_\lambda(F_n, W_n)$ on the factors W_n and F_n .

3. Neural Topographic Factor Analysis

NTFA extends TFA to model variation across participants and stimuli. We assume the same factor analysis model as TFA, which approximates the fMRI signal as a linear combination of time-dependent weights and spatially varying Gaussian factors. NTFA extends TFA by inferring *embedding vectors* for individual participants and stimuli. We learn a mapping from embeddings to the parameters of the likelihood model, parameterized by a neural network. Instead of HTFA’s global template, we introduce factorized latent spaces of participant and stimulus embeddings, and share the neural networks mapping embeddings to factors.

The advantage of incorporating neural networks into the generative model is that it enables us to explicitly reason about multimodal response distributions and effects that vary between individual samples. The network weights θ are shared across trials, as are the stimulus and participant embeddings z_s^S and z_p^P . This allows NTFA to capture statistical regularities within a whole experiment. At the same time, the use of neural networks ensures that differences in embeddings can be mapped onto a wide range of spatial and temporal responses. Whereas the hierarchical Gaussian priors in HTFA implicitly assume that response distributions are unimodal and uncorrelated across different factors $k \in [K]$, the neural network in NTFA is able to model such correlations by jointly predicting all K factors.

We model N trials in which participants $p_n \in \{1, \dots, P\}$ undergo a set of stimuli $s_n \in \{1, \dots, S\}$ and are scanned for T time points per trial. We assume that participant embeddings $\{z_1^P, \dots, z_P^P\}$ and stimulus embeddings $\{z_1^S, \dots, z_S^S\}$ are shared across trials. For simplicity, we will consider the case where both embeddings have the same dimensionality D and a Gaussian prior

$$z_p^P \sim \mathcal{N}(0, I), \quad z_s^S \sim \mathcal{N}(0, I). \quad (6)$$

For each participant p , we define the RBF center x_p^F and log-width ρ_p^F in terms of a neural mapping

$$x_p^F \sim \mathcal{N}(\mu_p^x, \sigma_p^x), \quad \mu_p^x, \sigma_p^x \leftarrow \eta_\theta^{F,x}(z_p^P), \quad (7)$$

$$\rho_p^F \sim \mathcal{N}(\mu_p^\rho, \sigma_p^\rho), \quad \mu_p^\rho, \sigma_p^\rho \leftarrow \eta_\theta^{F,\rho}(z_p^P). \quad (8)$$

Here η_θ^F is a neural network parameterized by a set of weights θ , which models how variations between participants and stimuli affect the factor positions and widths in brain activations. This network outputs a $K \times 4 \times 2$ tensor, that contains a 4-tuple of 2-dimensional parameters for

Algorithm 1 NeuralTFA Generative Model

| | |
|---|------------------------------|
| (p_1, \dots, p_N) | ▷ Participant for each trial |
| (s_1, \dots, s_N) | ▷ Stimulus for each trial |
| 1: for p in $1, \dots, P$ do | |
| 2: $z_p^p \sim \mathcal{N}(0, I)$ | ▷ Equation (6) |
| 3: $(\mu_p^x, \sigma_p^x), (\mu_p^\rho, \sigma_p^\rho) \leftarrow \eta_\theta^F(z_p^p)$ | |
| 4: $x_p^F \sim \mathcal{N}(\mu_p^x, \sigma_p^x)$ | ▷ Equation (7) |
| 5: $\rho_p^F \sim \mathcal{N}(\mu_p^\rho, \sigma_p^\rho)$ | ▷ Equation (8) |
| 6: for s in $1, \dots, S$ do | |
| 7: $z_s^s \sim \mathcal{N}(0, I)$ | ▷ Equation (6) |
| 8: for n in $1, \dots, N$ do | |
| 9: $p, s \leftarrow p_n, s_n$ | |
| 10: $\mu_n^w, \sigma_n^w \leftarrow \eta_\theta^W(z_p^p, z_s^s)$ | ▷ Equation (9) |
| 11: for t in $1 \dots T$ do | |
| 12: $W_{n,t} \sim \mathcal{N}(\mu_n^w, \sigma_n^w)$ | ▷ Equation (9) |
| 13: $F_p \leftarrow \kappa(x_p^F, \rho_p^F)$ | |
| 14: $Y_{n,t} \sim \mathcal{N}(W_{n,t} \cdot F_p, \sigma^Y)$ | ▷ Equation (10) |

each factor: $(\mu_{n,k}^w, \sigma_{n,k}^w, x_{n,k}^F, \log \rho_{n,k}^F)$. We use a second network $\eta_\theta^W(z_p^p, z_s^s)$ to parameterize the distribution over weights $W_{n,t}$ with a $K \times 2$ tensor, given the embeddings for each trial n and time point t with $p = p_n, s = s_n$:

$$W_{n,t} \sim \mathcal{N}(\mu_n^w, \sigma_n^w), \quad \mu_n^w, \sigma_n^w \leftarrow \eta_\theta^W(z_p^p, z_s^s). \quad (9)$$

The likelihood model is the same as that in TFA,

$$Y_{n,t} \sim \mathcal{N}(W_{n,t} \cdot F_p, \sigma^Y), \quad F_p \leftarrow \kappa(x_p^F, \rho_p^F). \quad (10)$$

We summarize the generative model for NTFA in Algorithm 1. This model defines a joint density $p_\theta(Y, W, x^F, \rho^F, z^P, z^S)$, which in turn defines a posterior $p_\theta(W, x^F, \rho^F, z^P, z^S \mid Y)$ when conditioned on Y . We approximate the posterior with a variational distribution,

$$q_\lambda(W, \rho^F, x^F, z^P, z^S) = \prod_{n,t} q_{\lambda_{n,t}^w}(W_{n,t}) \prod_s q_{\lambda_s^s}(z_s^S) \prod_p q_{\lambda_{x_p^F}}(x_p^F) q_{\lambda_{\rho_p^F}}(\rho_p^F) q_{\lambda_p^z}(z_p^P). \quad (11)$$

We learn the parameters θ and λ by maximizing the evidence lower bound (ELBO)

$$\mathcal{L}(\theta, \lambda) = \mathbb{E}_q \left[\log \frac{p_\theta(Y, W, x^F, \rho^F, z^P, z^S)}{q_\lambda(W, x^F, \rho^F, z^P, z^S)} \right] \leq \log p_\theta(Y).$$

We optimize this objective using black-box methods provided by Probabilistic Torch, a library for deep generative models that extends the PyTorch deep learning framework (Narayanaswamy et al., 2017). Specifically, we maximize an importance-weighted bound (Burda et al., 2016) using a doubly-reparameterized gradient estimator (Tucker et al., 2019). This objective provides more accurate estimates for the gradient of the log marginal likelihood.

While neural network models can have thousands or even millions of parameters, we emphasize that NTFA in fact has a *lower* number of trainable parameters than HTFA. This follows from the fact that TFA and HTFA assume fully-factorized variational distributions that have $O(NK + NTK)$ parameters for N trials with T time points. In NTFA, the networks η^F and η^W have $O(D(D + K))$ parameters each, whereas the variational distribution has $O(D(P + S) + PK + NTK)$ parameters.

In practice, scanning time limitations impose a trade-off between N and T . For this reason NTK does not always dominate NK , since often $T \propto O(10)$. We can then choose $D \propto O(1)$ and $K \propto O(100)$, and if we label constant factors c , the total number of parameters becomes $O(cD^2 + cDK)$, making $O(cDK)$ the dominant term. When $P \ll N$, as is usually the case, NTFA can therefore have orders of magnitude fewer parameters than HTFA for $D = 2$.

4. Experiments

4.1. Datasets

We consider four datasets in our experiments. First, we create a simulated dataset to verify that NTFA can recover a ground-truth structure in data that, by construction, contains clearly distinguishable participant and stimulus clusters. Second, we analyze a previously unpublished data from a pilot study, conducted by one of the authors, that measures the neural response to threat-relevant stimuli. Third, we analyze a publicly available dataset on valenced sounds and music, with participants divided into a control group and a depressed group (Lepping et al., 2016). Finally, we verify that NTFA can reconstruct a second publicly available dataset used to evaluate numerous fMRI analyses (Haxby et al., 2001). These experimental datasets vary in their number of participants, time points, and voxels, as well as task variables.

Synthetic Data: We consider a simulated dataset in which there are three participant groups (*Group 1*, *Group 2* and *Group 3*) of five participants each. All participants underwent two categories of hypothetical stimuli, called *Task 1* and *Task 2*, with five stimuli within each category. Each participant underwent one hypothetical scanning run with rest trials interleaved between stimuli. We manually defined three distinct factors in a standard MNI_152.8mm brain. We then sampled participant embeddings $\{z_1^p, \dots, z_{15}^p\}$ and stimulus embeddings $\{z_1^s, \dots, z_{10}^s\}$, from mixtures of three and two distinct Gaussians respectively. We set the means for these Gaussians to meet the following conditions under noisy combination. **1.** All participants show no whole-brain response during rest except random noise. **2.** Under *Task 1* stimuli, Group 1 exhibits approximately half the response in the first region as compared to under *Task 2* stimuli. The rest of the brain shows no response. Similarly, Group 2 and Group 3 exhibit a response in the second and third regions

Table 1. Parameter counts: For embeddings with dimensionality $D = 2$, NTFA has 30% fewer parameters on the Haxby dataset, and orders of magnitude fewer parameters for other datasets, which have many more trials than participants ($N \gg P$). In both models we use $K = 100$ factors for all datasets.

| Dataset | HTFA parameters | NTFA parameters |
|-----------------------|--------------------|--------------------|
| Haxby | 1.44×10^6 | 1.01×10^6 |
| Lepping | 2.53×10^7 | 2.61×10^6 |
| ThreatVids | 1.64×10^8 | 8.88×10^6 |
| Synthetic ($K = 3$) | 2.16×10^4 | 1.90×10^4 |

respectively, while the rest of the brain shows no response. **3.** Each stimulus in *Task 1* and *Task 2* provokes a response lower or higher than the stimulus category’s average based on the stimulus embedding’s location. Pseudocode detailing the generation of this dataset is included in Appendix A.4.

Threat Videos (“ThreatVids”)²: A fundamental question in affective neuroscience is whether threat-relevant stimuli from different categories involve a single or multiple distinct systems (Wager et al., 2015). To evaluate whether NTFA can provide insight into this fundamental research question, we conducted and analyzed our own study. 21 participants each watched 36 videos depicting threat-related content involving spiders, looming heights, and social evaluative threat (12 videos per category). Each video was approximately 20 seconds long and was followed by a set of self-report ratings and a rest period. The videos were chosen to vary in how much fear they normatively evoke within each category. This data contains 81,638 voxels (white matter removed) and 552 time points per scanning run for three runs. Using NTFA, we examine whether neural activity justified organization of the stimuli into three categories.

Emotional Musical and Nonmusical Stimuli in Depression (“Lepping”) (Lepping et al., 2016)³: 19 participants with major depressive disorder and 20 control participants (P=39) underwent emotional musical and nonmusical stimuli to examine neural processing of emotionally provocative auditory stimuli in depression. Each run consisted of trials in which participants listened to music or nonmusical valenced (positive or negative) sounds, interleaved with trials in which they heard neutral tones. The fMRI data had 62,733 voxels (white matter removed) and 105 time points in each scanning run for five runs.

Face and Objects Image Viewing (“Haxby”) (Haxby et al., 2001)⁴: fMRI was used to measure whole brain re-

²This dataset is currently in preparation for online repository pending deidentification and submission of an empirical report.

³This data was obtained from the OpenfMRI database. Its accession number is ds000171.

⁴<https://openneuro.org/datasets/ds000105/>

Table 2. Generalization performance in terms of log posterior-predictive probability. We approximate the log posterior predictive with a VAE-style lower bound. We evaluate on a test set of held out subject-stimuli pairs.

| | HTFA | NTFA |
|---|---------------------|---------------------|
| Log posterior predictive (VAE bound, test set) | | |
| Synthetic ($K = 3$) | -4.72×10^6 | -4.68×10^6 |
| ThreatVids | -7.04×10^7 | -4.40×10^7 |
| Lepping | -1.72×10^8 | -8.52×10^7 |
| Haxby | -4.70×10^7 | -2.40×10^7 |

sponse while subjects viewed faces, cats, five categories of man-made objects, and scrambled pictures. The study consisted of six subjects (P=6) and 12 scanning runs per subject, with 32,233 voxels (white matter removed) and 121 time points for each scanning run.

4.2. Preprocessing

The raw BOLD signal collected in fMRI is generally not usable for analysis. It contains both physiological (cerebrospinal fluids, global signal, and white matter) and motion artifacts. We employ standard neuroimaging preprocessing - including slice timing correction, high pass filtering and spatial smoothing - for all fMRI data using fMRIPrep (Esteban et al., 2019). The processed data still has units that are not comparable across scanning runs. For the ThreatVids and Haxby datasets, we z-scored each task trial with respect to the entire set of rest trials (trials in which no stimulus was presented) within each run. For the Lepping dataset, we treated the trials with neutral tones as rest trials and performed the same z-scoring procedure. This converts the data to a common scale of units across trials within a dataset, capturing meaningful difference in activation intensities relative to neutral conditions (“rest” and “tones”). Since neural activity peaks about three seconds after the task onset (Aguirre et al., 1998), we make sure to account for this delay when loading each dataset by offsetting the stimulus onsets by three seconds. We input the resulting z-scored data to NTFA, and use it for all evaluations.

4.3. Model Architecture and Training

We employ participant and stimulus embeddings of dimensions $D = 2$ in all experiments for simplicity and ease of visualization. For the synthetic dataset, we analyze the data with the same number of factors as were used to generate it, $K = 3$. In contrast to our work on NTFA, previous work on models such as HTFA has used factor counts as high as $K=700$ in order to hit an arbitrarily fixed mean (over voxels and timepoints) squared reconstruction error (Manning et al., 2018). To mitigate the risk of overfitting, we employ $K = 100$ factors for our real datasets. We report parameter counts for HTFA and NTFA in Table 4.1. Architectural details for our neural networks are given in Appendix A.2.

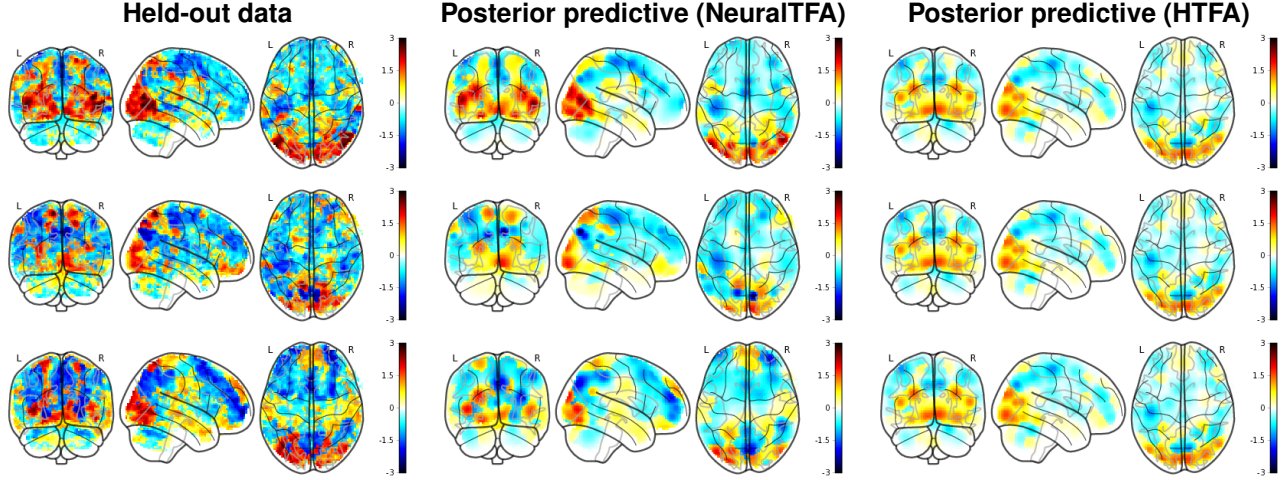


Figure 2. **Predictive distribution for the ThreatVids dataset:** We compare time-averaged held-out data (*left*) to the posterior-predictive mean for three trials. In NTFA (*center*), the learned generative model and inferred embeddings inform the distribution for unseen participant-stimulus combinations. In HTFA (*right*) the predictive distribution is the same for trials, since the shared global template in this model does not differentiate between participants and stimuli.

We train the parameters θ and λ on all models using the Adam optimizer (Kingma & Ba, 2015) for 1000-1500 epochs per dataset. We use one particle to calculate the IWAE bound to the log-evidence and its gradient estimator at training time, with a learning rate $\eta_\lambda = 0.01$ and $\eta_\theta = 0.0001$. We anneal the learning rate with a patience of 100 epochs, and a multiplicative decline of 0.5. This only affects convergence on the synthetic dataset.

5. Evaluation

5.1. Generalization to Held-out Images

To evaluate generalization, we split datasets into training and test sets in a manner that ensures the training set contains at least one trial for each participant $p \in \{1, \dots, P\}$ and each stimulus $s \in \{1, \dots, S\}$. To do so, we construct a matrix of $(p, s) \in \{1, \dots, P\} \times \{1, \dots, S\}$ with participants as rows and stimuli as columns. We then choose all trials along the matrix’s diagonals $\{n : p_n \bmod S = s_n\}$ as our test set. All other trials are used as the training set.

We evaluate generalization to held-out data in terms of the posterior-predictive probability

$$p_\theta(\tilde{Y} | Y) = \int p_\theta(\tilde{Y} | z^p, z^s) p_\theta(z^p, z^s | Y) dz^p dz^s.$$

Like the marginal likelihood, this quantity is intractable. We approximate it by computing a VAE-style lower bound $\mathbb{E}[\tilde{\mathcal{L}}] \leq \log p_\theta(\tilde{Y} | Y)$ from L samples,

$$\tilde{\mathcal{L}} = \frac{1}{L} \sum_{l=1}^L \log p(\tilde{Y} | \tilde{W}^{(l)}, \tilde{x}^F{}^{(l)}, \tilde{\rho}^F{}^{(l)}, z^p{}^{(l)}, z^s{}^{(l)}). \quad (12)$$

We sample embeddings from the variational distribution

$$z^p{}^{(l)} \sim q(z^p), \quad z^s{}^{(l)} \sim q(z^s),$$

and remaining variables from the learned generative model

$$\tilde{W}^{(l)}, \tilde{x}^F{}^{(l)}, \tilde{\rho}^F{}^{(l)} \sim p_\theta(\tilde{W}, \tilde{x}^F, \tilde{\rho}^F | z^p{}^{(l)}, z^s{}^{(l)}).$$

For a full derivation of this bound, see Appendix A.6.

To visualize the predictive distribution, we compare the time-average of \tilde{Y} to a prediction $\bar{Y} = \bar{\mu}^w \cdot \kappa(\bar{\mu}_p^x, \bar{\mu}_p^p)$, where $\bar{\mu}^w, \bar{\mu}_p^x, \bar{\mu}_p^p$ are computed from the expected values \bar{z}^p and \bar{z}^s of the embeddings in the variational distribution.

In Table 2, we compare NTFA to HTFA in terms of the log posterior-predictive probability for held-out data. We compute an importance-weighted bound to the log-predictive probability for each dataset’s test set.

Across datasets, NTFA exhibits a higher log-likelihood and log-predictive probability than HTFA, with the same number ($K = 100$) of latent factors. Improvements relative to HTFA are smallest in the synthetic dataset, which comprises images that contain a small number of factors and white noise. In contrast, we observe larger improvements by NTFA over HTFA in datasets such as ThreatVids, in which the fact that $N \gg P$ and $N \gg S$ enables our generative model to share statistical strength across trials.

In Figure 2 we visualize the posterior-predictive mean for three held-out trials from the ThreatVids dataset. In HTFA, which lacks an explicit representation of participant and stimuli, the posterior predictive is the same in all trials. By contrast, the predictive distribution in NTFA varies across trials and better represents the actual data. Similar visualizations for other datasets are shown in Appendix A.5.

5.2. Inferred Embeddings

NTFA infers embeddings for both participants and stimuli. Here we discuss how stimulus embeddings map to

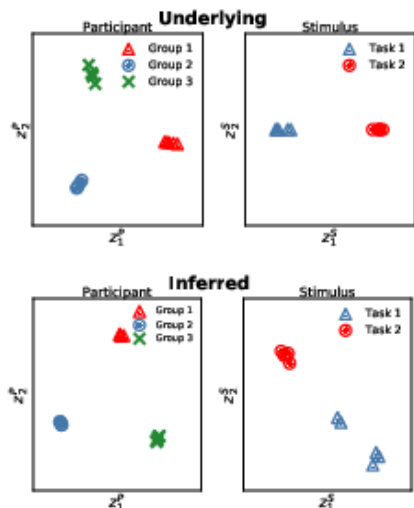


Figure 3. Inferred embeddings for synthetic data: In the simulated data, three groups of participants exhibit varying levels of response in three different brain regions to *Task 1* and *Task 2* stimuli, depending on the locations of underlying participant and stimulus embeddings used to generate the data (top). Without prior knowledge of participant groups and stimulus categories, NTFA recovers these conditions in participant and stimulus embeddings (bottom). Only the relative spatial arrangement is of interest.

experimenter-defined categories, before considering downstream classification tasks. Participant embeddings appeared to primarily reflect idiosyncratic differences among participants, without mapping clearly to any participant conditions or behavior available in the datasets. We discuss these participant embeddings in detail in Appendix A.1.

Synthetic Data: For synthetic data, NTFA recovers stimulus and participant embeddings that are qualitatively very similar to the embeddings that we used to generate the data (Figure 3). We emphasize that embeddings are learned directly from the synthetic data in an entirely unsupervised manner, which means that there is in principle no reason to expect embeddings to be exactly the same. However, we do observe that learned embeddings for participants and stimuli are well-separated, appear to have some variance, and are invariant under linear transformations. Moreover, given the “true” number of factors ($K = 3$), NTFA reconstructs synthetic data better than HTFA.

ThreadVids Dataset: In this dataset, metadata provided individual stimulus labels as well as stimulus categories to group them together. Figure 2 shows that NTFA successfully generalizes to participant-stimulus pairs on which it was not trained, without additional inference. In an analysis without resting-state data, NTFA uncovers stimulus embeddings that clearly correlate with stimulus categories. While “Heights” and “Spiders” show some overlap, “Social Threat” is clearly separated (Figure 4, left column).

Lepping Dataset: The supplied metadata labeled stimuli

by category rather than individually, and so NTFA could only acquire one embedding for each stimulus category. However, the embeddings (Figure 4, middle column) display a clear separation between music and nonmusical sounds, with positive and negative music being relatively easier to differentiate from each-other. Positive and negative sounds appear virtually indistinguishable in the embedding space, consistent with the original findings of Lepping et al. (2016).

Haxby Dataset: The supplied metadata labeled stimuli by category rather than individually. Inference resulted in stimulus embeddings that varied roughly linearly, while exhibiting minor variation in the vertical dimension (Figure 4, right column). These embeddings reflect the evidence for distinct processing of animate and inanimate objects in scenes (Naselaris et al., 2012; Blumenthal et al., 2018), with embeddings for faces and cats lying opposite to those for houses.

5.3. Traditional Neuroscientific Analyses

One of the advantages of learning a deep generative model is that we can use the learned latent representations in downstream tasks. To illustrate this use case, we consider two types of post-scan analyses that are commonly performed on full fMRI data. As features in these analyses we use the dimensionality-reduced representation learned by NTFA: the inferred factor locations, widths, and weights.

Multivoxel Pattern Analysis: In MVPA, a regularized linear classifier is trained to predict experimental variables from distributed patterns of mean voxel intensities, this is usually preceded by a supervised feature selection step to select voxels most relevant to the classification task (Pereira et al., 2009). We perform this standard method on our datasets and compare it to using means (over time) of the weight matrices from NTFA and HTFA instead of the supervised feature selection step. We show the resulting classification accuracy scores, measured using Area Under the (receiver operating) Curve on the left in Figure 5. While all three methods perform significantly better than chance, NTFA outperforms HTFA, and performs almost as well as supervised voxel selection. We also note that the stimulus embeddings qualitatively predict classification performance on different stimulus categories, as seen in the middle of Figure 5 for Lepping dataset. NTFA learns a latent factor representation useful for different MVPA stimulus classification tasks, without supervised feature selection. We detail the methods and results in Appendix A.3.

Functional Connectivity (FC): Functional connectivity analyses are used to study the co-activation of brain areas during resting-state or during a task, regardless of their apparent physical distance. FC, and changes in FC, have been shown to correlate with behavior in a variety of settings (Elliott et al., 2019). Voxels, however, capture neither single neurons for cellular-scale analyses, nor functional brain

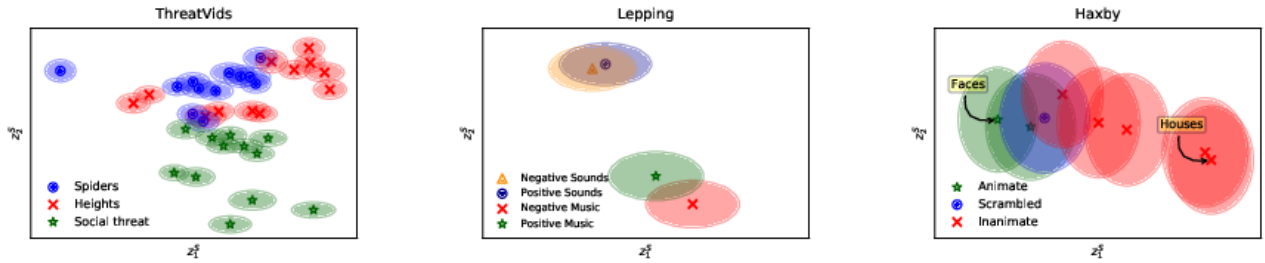


Figure 4. **Inferred stimulus embeddings for ThreatVids, Lepping, and Haxby datasets.** Markers and ellipses indicate the mean and covariance of the variational distribution. **Left:** On ThreatVids, stimulus embeddings recovered groups of fear stimuli. **Middle:** On the Lepping dataset, stimulus embeddings clearly distinguish the musical stimuli from the non-musical sounds; moreover, positive and negative music show less overlap than positive and negative sounds, consistent with the previously reported finding that the valence effect is marginally stronger in the musical stimuli as compared to non-musical stimuli (Lepping et al., 2016). **Right:** On the Haxby dataset, stimulus embeddings for faces and cats (animate objects) are separated from various inanimate objects by the embedding for scrambled pictures, reflecting evidence for distinct processing of animate and inanimate stimuli (Naselaris et al., 2012; Blumenthal et al., 2018). Faces were among the animate embeddings and clearly distinct from the embedding for houses, as expected (Haxby et al., 2001).

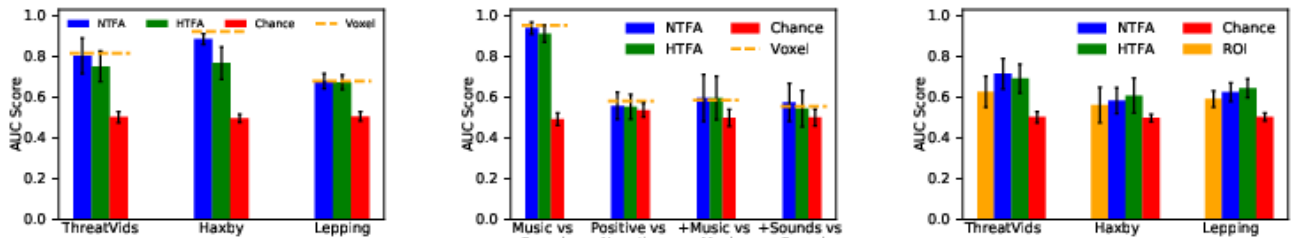


Figure 5. **Classification performance** measured using Area Under the (receiver operating) Curve (AUC). **Left:** For each dataset, we show the average performance of a traditional method of supervised voxel selection followed by a linear SVM (Pereira et al., 2009) as the orange lines labelled “Voxel”, across primary stimulus categories for each subject. We also show the means and 95% confidence intervals of the average scores for each subject when using NTFA and HTFA instead of the supervised voxel selection. Both NTFA and HTFA performed significantly above chance, with NTFA performing almost as well as supervised voxel selection. **Middle:** Classification performance on the Lepping dataset across different stimulus categories. The stimulus embeddings shown in the middle of Figure 4 qualitatively predict better classification for music vs sounds as compared to other possible task classifications. **Right:** The same classification pipeline, but using pairwise correlation matrices calculated across time. For the raw voxel data, we use a standard Region of Interest (ROI) parcellation from the Human Connectome Project (Glasser et al., 2016). The data-driven functional connectomes derived from the weight matrices from NTFA and HTFA’s factors outperform the data-agnostic ROIs.

regions that could hypothetically share an activation pattern. Standard Regions of Interest (ROIs) can divide the brain in a data-agnostic way. NTFA’s latent factor representations provide a data-driven alternative.

In Figure 5 (rightmost column), we see that linear classifiers trained on NTFA’s latent factor representation perform better than those trained on ROIs at a stimulus classification task. NTFA-derived FC patterns perform comparably to those derived from HTFA, but NTFA requires fewer parameters and shares statistical strength across trials.

6. Discussion

We have introduced Neural Topographic Factor Analysis, an unsupervised model for fMRI data that characterizes individual variation in the neural response by inferring low-dimensional embeddings for participants and stimuli.

NTFA recovers ground-truth structure in simulated data, and achieves state of the art log-predictive probabilities for unseen participant-stimulus combinations in three fMRI datasets. For two existing datasets, the locations of inferred stimuli embeddings align with prior findings about variation in the neural response across stimulus categories. Analysis of a pilot study conducted by the authors shows that stimuli group into categories, albeit with some overlap. Moreover, NTFA learns a feature representation, without supervision, that achieves competitive performance in downstream tasks relative to traditional supervised feature selection methods.

More generally, NTFA is a first step in a line of approaches that employ deep generative models as a means of incorporating inductive biases into unsupervised analyses of neuroimaging experiments. By designing models whose structure reflects a particular experimental design, or potentially even a neuroscientific hypothesis, we can hope to appropri-

ately account for the uncertainties that arise from limitations in statistical power. This provides a path towards analyses that reason about individual variation in a manner that is data-efficient and mitigate risks of overfitting to the data.

References

- Abdi, H. and Williams, L. J. Principal component analysis. *Wiley interdisciplinary reviews: computational statistics*, 2(4):433–459, 2010.
- Abraham, A., Pedregosa, F., Eickenberg, M., Gervais, P., Mueller, A., Kossaifi, J., Gramfort, A., Thirion, B., and Varoquaux, G. Machine learning for neuroimaging with scikit-learn. *Frontiers in neuroinformatics*, 8:14, 2014.
- Aguirre, G. K., Zarahn, E., and D’esposito, M. The variability of human, bold hemodynamic responses. *Neuroimage*, 8(4):360–369, 1998.
- Blumenthal, A., Stojanoski, B., Martin, C. B., Cusack, R., and Khler, S. Animacy and real-world size shape object representations in the human medial temporal lobes. *Human Brain Mapping*, 39(9):3779–3792, 2018. doi: 10.1002/hbm.24212. URL <https://onlinelibrary.wiley.com/doi/abs/10.1002/hbm.24212>.
- Burda, Y., Grosse, R., and Salakhutdinov, R. Importance Weighted Autoencoders. In *International Conference on Learning Representations*, 2016. URL <http://arxiv.org/abs/1509.00519>.
- Elliott, M. L., Knodt, A. R., Cooke, M., Kim, M. J., Melzer, T. R., Keenan, R., Ireland, D., Ramrakha, S., Poulton, R., Caspi, A., Moffitt, T. E., and Hariri, A. R. General functional connectivity: Shared features of resting-state and task fMRI drive reliable and heritable individual differences in functional brain networks. *NeuroImage*, 189:516–532, 2019. ISSN 10959572. doi: 10.1016/j.neuroimage.2019.01.068.
- Esteban, O., Markiewicz, C. J., Blair, R. W., Moodie, C. A., Isik, A. I., Erramuzpe, A., Kent, J. D., Goncalves, M., DuPre, E., Snyder, M., et al. fmriprep: a robust preprocessing pipeline for functional mri. *Nature methods*, 16(1):111–116, 2019.
- Gershman, S. J., Blei, D. M., Pereira, F., and Norman, K. A. A topographic latent source model for fmri data. *NeuroImage*, 57(1):89–100, 2011.
- Gershman, S. J., Blei, D. M., Norman, K. A., and Sederberg, P. B. Decomposing spatiotemporal brain patterns into topographic latent sources. *NeuroImage*, 98:91–102, 2014. ISSN 10959572. doi: 10.1016/j.neuroimage.2014.04.055.
- Glasser, M. F., Coalson, T. S., Robinson, E. C., Hacker, C. D., Harwell, J., Yacoub, E., Ugurbil, K., Andersson, J., Beckmann, C. F., Jenkinson, M., et al. A multi-modal parcellation of human cerebral cortex. *Nature*, 536(7615): 171–178, 2016.
- Haxby, J. V., Gobbini, M. I., Furey, M. L., Ishai, A., Schouten, J. L., and Pietrini, P. Distributed and Overlapping Representations of Faces and Objects in Ventral Temporal Cortex. *Science*, 293(5539):2425–2430, 2001. ISSN 0036-8075. doi: 10.1126/science.1063736. URL <https://science.sciencemag.org/content/293/5539/2425>.
- Haxby, J. V., Guntupalli, J. S., Connolly, A. C., Halchenko, Y. O., Conroy, B. R., Gobbini, M. I., Hanke, M., and Ramadge, P. J. A common, high-dimensional model of the representational space in human ventral temporal cortex. *Neuron*, 72(2):404–416, 2011.
- Hyvärinen, A., Karhunen, J., and Oja, E. *Independent Component Analysis*. Wiley Online Library, 2001.
- Kingma, D. P. and Ba, J. Adam: A Method for Stochastic Optimization. In *International Conference on Learning Representations*, pp. 1–15, 2015. URL <http://arxiv.org/abs/1412.6980>.
- Lepping, R. J., Atchley, R. A., Chrysiou, E., Martin, L. E., Clair, A. A., Ingram, R. E., Simmons, W. K., and Savage, C. R. Neural processing of emotional musical and nonmusical stimuli in depression. *PLOS ONE*, 11(6):1–23, 06 2016. doi: 10.1371/journal.pone.0156859. URL <https://doi.org/10.1371/journal.pone.0156859>.
- Manning, J. R., Ranganath, R., Keung, W., Turk-Browne, N. B., Cohen, J. D., Norman, K. A., and Blei, D. M. Hierarchical topographic factor analysis. In *Pattern Recognition in Neuroimaging, 2014 International Workshop On*, pp. 1–4. IEEE, 2014a.
- Manning, J. R., Ranganath, R., Norman, K. A., and Blei, D. M. Topographic Factor Analysis: A Bayesian Model for Inferring Brain Networks from Neural Data. *PLOS ONE*, 9(5):e94914, May 2014b. ISSN 1932-6203. doi: 10.1371/journal.pone.0094914.
- Manning, J. R., Zhu, X., Willke, T. L., Ranganath, R., Stachenfeld, K., Hasson, U., Blei, D. M., and Norman, K. A. A probabilistic approach to discovering dynamic full-brain functional connectivity patterns. *NeuroImage*, 2018.
- Narayanaswamy, S., Paige, T. B., van de Meent, J.-W., Desmaison, A., Goodman, N., Kohli, P., Wood, F., and Torr, P. Learning Disentangled Representations with

Semi-Supervised Deep Generative Models. In Guyon, I., Luxburg, U. V., Bengio, S., Wallach, H., Fergus, R., Vishwanathan, S., and Garnett, R. (eds.), *Advances in Neural Information Processing Systems 30*, pp. 5927–5937. Curran Associates, Inc., 2017.

Naselaris, T., Stansbury, D. E., and Gallant, J. L. Cortical representation of animate and inanimate objects in complex natural scenes. *Journal of Physiology-Paris*, 106(5):239 – 249, 2012. ISSN 0928-4257. doi: <https://doi.org/10.1016/j.jphysparis.2012.02.001>. URL <http://www.sciencedirect.com/science/article/pii/S092842571200006X>. New trends in neurogeometrical approaches to the brain and mind problem.

Pereira, F., Mitchell, T., and Botvinick, M. Machine learning classifiers and fMRI: a tutorial overview. *NeuroImage*, 45(1 Suppl):S199–S209, 2009. ISSN 10959572. doi: 10.1016/j.neuroimage.2008.11.007. URL <http://dx.doi.org/10.1016/j.neuroimage.2008.11.007>.

Tucker, G., Lawson, D., Gu, S., and Maddison, C. J. Doubly Reparameterized Gradient Estimators for Monte Carlo Objectives. In *International Conference on Learning Representations*, pp. 1–12, 2019. URL <http://arxiv.org/abs/1810.04152>.

Wager, T. D., Kang, J., Johnson, T. D., Nichols, T. E., Satpute, A. B., and Barrett, L. F. A bayesian model of category-specific emotional brain responses. *PLoS computational biology*, 11(4), 2015.

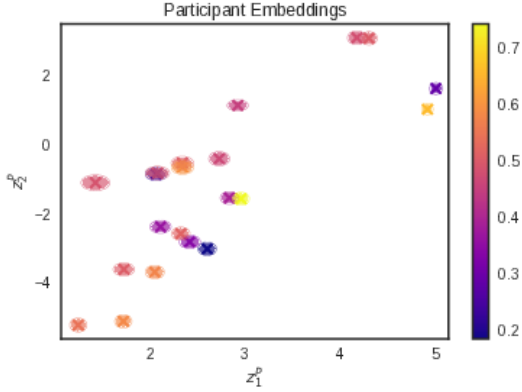


Figure 6. Participant embeddings from the ThreatVids dataset. Crosses indicate the location of the (approximate) posterior mean, and ellipses display (approximate) posterior covariance. The labels are used only for visualization purposes. Participant embeddings are color-coded by their reported level of fear across all stimulus categories (heights, spiders, and social threats). Cooler colors indicate lower mean fear ratings, while warmer colors indicate higher mean fear ratings.

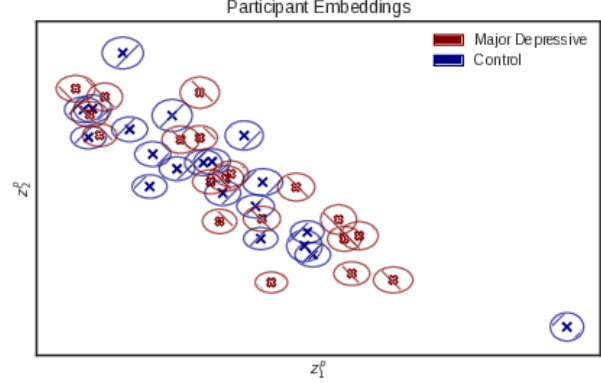


Figure 7. Participant embeddings for the Lepping dataset (Lepping et al., 2016). Crosses indicate the location of the posterior mean, and ellipses display posterior covariance. The labels are used only for visualization purposes. Participant embeddings did not show a clear difference between control and major depressive groups, but did appear scattered around a linear trend in the latent space, which we have yet to interpret.

A. Appendix

A.1. Participant embedding results

In the ThreatVids dataset, the participant embeddings uncovered three groups: the more frightened, the less frightened, and those sensitive to particular fears (Figure 6). Participant embeddings for individual fear categories are shown in Figure 6. Participants were not recruited in specific groups (e.g. arachnophobes and acrophobes), and stimuli could be categorized multiple ways (e.g. by kind or degree). We observe that most participants carried a greater fear of heights (left) and social threat (right) than of spiders (middle). A scattering of individuals in the mid-left of the embedding space appeared to suffer little overall fear in any stimulus category, while those further out from the centroid had more varied fear experiences across categories. Few individuals showed high mean fear ratings across stimulus categories.

The participant embeddings do not seem to predict the self-reported fear ratings. However as shown in Figure 6 they do seem to uncover variations among participants in the latent space. Note, for example the participant groups breaking away from the central “cluster” towards top-right and bottom-left. This suggests that there are factors not explained by the self-reported fear ratings that might be driving the individual variation in response among participants.

Table 3. Network architectures for η_{θ}^F and η_{θ}^W

| Layer | $p_{\theta}(x_p^F, \rho_p^F z_p^p)$ | $p_{\theta}(W_{n,t} z_p^p, z_s^s)$ |
|--------|--|---|
| Input | $z_p^p \in \mathbb{R}^D$ | $z_p^p, z_s^s \in \mathbb{R}^D$ |
| 1 | FC $D \times 2D$ PReLU | FC $2D \times 4D$ PReLU |
| 2 | FC $2D \times 4D$ PReLU | FC $4D \times 8D$ PReLU |
| 3 | FC $4D \times 8K$ | FC $8D \times 2K$ |
| Output | $(\mu_p^x, \sigma_p^x, \mu_p^{\rho}, \sigma_p^{\rho}) \in \mathbb{R}^{8K}$ | $(\mu_n^w, \sigma_n^w) \in \mathbb{R}^{2K}$ |

A.2. Neural network architectures and initialization

The network $\eta_{\theta}^F(\cdot)$ is a multilayer perceptron (MLP) with one hidden layer and PReLU activations. We extract the factor parameters F, x and F, ρ by viewing the $8K$ -dimensional result as a $K \times 4 \times 2$ tensor. The network $\eta_{\theta}^W(\cdot)$ is similarly an MLP with one hidden layer, though operating over both embeddings. We extract the weight parameters W_n by casting its $2K$ -dimensional result as a $K \times 2$ matrix. Architectural details for both networks are given in Table 3. The neural network weights θ specify the linear layers of the networks.

Similarly to Manning et al. (2018), we employ a K-means initialization in all experiments across models, initializing the variational parameters for HTFA and the bias in the final layer of the generative model for NTFA.

A.3. MVPA Classification

In this section we provide details of the classification pipeline as well as results beyond those presented in Figure 5. The traditional pipeline outlined in Pereira et al. (2009) was used to do classification on the input data. One classical

approach is to first select a subset of voxels with reliably different mean intensities between the experimental variables being tested. Usually this is done by selecting 500 voxels based on the f -statistic from an analysis of variance (ANOVA). After this supervised feature selection step, a linear support-vector machine (SVM) is usually trained (without hyperparameter tuning) over some combination of cross-validation scans.

For each block (an instance of a participant undergoing a stimulus), only the mean voxel activity was considered. We employed a leave-out-one cross-validation approach with respect to scanning runs for each subject, with a one-vs-all linear SVM trained and tested for each stimulus category. For Haxby and ThreatVids, we used a leave-one-out cross-validation approach on scanning runs, while for Lepping (in which the experimental design did not support leaving whole scanning sessions out) we applied a stratified three-fold cross-validation scheme across all trials with the same stimulus. We then ran the same classification pipeline again, substituting NTFA’s and HTFA’s MAP estimates of the weight matrix W for the label-supervised voxels.

For each cross validation run, the feature selection of voxels was done by keeping the top 500 of the voxels with the most reliable differences in the mean intensity for the stimulus category the classifier was being trained for vs the remaining categories. The linear SVM trained on these selected voxels on training runs was then tested on the held-out runs. Since this is a one-vs-all scheme, the classes are unbalanced, and raw accuracy can be inflated just by predicting the most frequent class. We therefore report Area Under the ROC Curve (AUC) instead.

For NTFA and HTFA, we use the same pipeline, except there is no supervised feature selection step. Instead, we used MAP estimates of generated $W \in \mathbb{R}^{T \times K}$ matrices, averaged across time. These were employed as the training features for classifiers with respect to the cross-validation scheme above. As is evident from Figure 5, and Tables 4 and 5, NTFA performs similarly to the supervised pipeline above, and often outperforms HTFA.

A.4. Synthetic data generation

Algorithm 2 shows the procedure for generating synthetic datasets similar to the synthetic data used in this paper. We will also include the exact script with the code repository for our method.

A.5. Test-set predictions for additional datasets

Here we show test predictions from both NTFA and HTFA for our two other real datasets, Lepping (Figure 8) and Haxby (Figure 9). HTFA’s pale experiment-wide averages on the Lepping dataset show its inability to capture the

Algorithm 2 Generating a simple Synthetic data to test NTFA using Nilearn (Abraham et al., 2014)

```

Load Template Brain           ▷ e.g. MNI152_8mm
Define dataset parameters: T=Number of time points
per block, K=Number of factors, C=Number of stimu-
lus categories,  $N_C$ =Number of stimuli per category,
 $G$ =Number of participant groups,  $N_G$ =Number of par-
ticipants per group.
Define means  $\mu_{1\dots C}^S$  and covariances  $\Sigma_{1\dots C}^S$  for em-
beddings for each stimulus category. Total Stimuli
 $S = C * N_C + (2N_C + 1)$  (to allow for interleaved rest
blocks) and Total Participants  $P = G * N_G$ 
Define means  $\mu_{1\dots G}^P$  and covariances  $\Sigma_{1\dots G}^P$  for embed-
dings each participant condition group.
Manually select  $K$  voxels in the template brain to be the
centers of the factors  $x_{1,\dots,K}^F$ . Define a gaussian noise
for factors with standard deviation  $\sigma^x$ . Also define
factor log widths  $\rho_{1,\dots,K}^F \sim \mathcal{N}(\mu^\rho, \sigma^\rho)$ . These together
define the matrix of Factors  $F$  through an RBF.
Order the total stimuli according to required experiment
design and save indices accordingly. e.g. Category 1,
Rest, Category 2, Rest, and so on.
1: for  $c$  in  $1, \dots, C$  do
2:   for  $s$  in  $1, \dots, N_C$  do  $z_s^c \sim \mathcal{N}(\mu_c^S, \Sigma_c^S)$ 
   ▷ generate stimulus embeddings
3: for  $g$  in  $1, \dots, G$  do
4:   for  $p$  in  $1, \dots, N_G$  do  $z_p^g \sim \mathcal{N}(\mu_g^P, \Sigma_g^P)$ 
   ▷ generate participant embeddings
5: for  $g$  in  $1, \dots, G$  do
6:   for  $p$  in  $1, \dots, N_G$  do
7:     for  $s$  in  $1, \dots, S$  do
8:       for  $k$  in  $1, \dots, K$  do
9:          $W_{[k,s:s+T]} \sim \mathcal{N}(0, \sigma^W)$    ▷ If  $s$  is the
         start of a rest block
10:         $W_{[k,s:s+T]} \sim \mathcal{N}(z_p^T z_s, \sigma^W)$ 
         $Y_{p+(g-1)*N_G} = WF$    ▷ data for one participant
    
```

participant- and stimulus-wise variations captured clearly by NTFA. While HTFA does make clear predictions for its average across the Haxby dataset, nonetheless, it does not capture the variation across trials that NTFA does.

A.6. Derivation of the lower bound to the log posterior predictive distribution

We begin by showing how to use the variational distribution to approximate the posterior predictive distribution via importance sampling, and then convert the resulting importance weight into a lower bound on the log posterior predictive. Posterior sampling from the NTFA generative model, conditioned upon the posterior distribution over em-

beddings, would yield the joint distribution

$$p(\tilde{Y}, \tilde{W}, \tilde{x}^F, \tilde{\rho}^F, z^P, z^S | Y) = p(\tilde{Y}, \tilde{W}, \tilde{x}^F, \tilde{\rho}^F | z^P, z^S) p(z^P, z^S | Y),$$

which factorizes according to the generative model as,

$$p(\tilde{Y}, \tilde{W}, \tilde{x}^F, \tilde{\rho}^F, z^P, z^S | Y) = p(\tilde{Y} | \tilde{W}, \tilde{x}^F, \tilde{\rho}^F, z^P, z^S) p(\tilde{W} | z^P, z^S) p(\tilde{x}^F, \tilde{\rho}^F | z^P) p(z^P, z^S | Y).$$

The marginal of this joint distribution, that being the posterior predictive distribution, can be defined by importance weighting, where the learned variational distributions $q(z^P)$, $q(z^S)$ serve as proposals for z^P and z^S while the generative model serves as its own proposal for the other latent variables, yielding

$$\begin{aligned} p(\tilde{Y} | Y) &= \mathbb{E}_{q,p} \left[\frac{p(\tilde{Y}, \tilde{W}, \tilde{x}^F, \tilde{\rho}^F, z^P, z^S | Y)}{p(\tilde{W}, \tilde{x}^F, \tilde{\rho}^F | z^P, z^S) q(z^P) q(z^S)} \right] \\ &= \mathbb{E}_{q,p} \left[\frac{p(\tilde{Y} | \tilde{W}, \tilde{x}^F, \tilde{\rho}^F, z^P, z^S) p(\tilde{W} | z^P, z^S)}{p(\tilde{W} | z^P, z^S)} \cdot \frac{p(\tilde{x}^F, \tilde{\rho}^F | z^P) p(z^P, z^S | Y)}{p(\tilde{x}^F, \tilde{\rho}^F | z^P) q(z^P) q(z^S)} \right] \\ &= \mathbb{E}_{q,p} \left[\frac{p(\tilde{Y} | \tilde{W}, \tilde{x}^F, \tilde{\rho}^F, z^P, z^S) p(z^P, z^S | Y)}{q(z^P) q(z^S)} \right]. \end{aligned}$$

We can then apply Jensen's inequality to define a lower bound

$$\begin{aligned} \text{ELBO}_{\tilde{Y}|Y} &= \mathbb{E}_{q,p} \left[\log \frac{p(\tilde{Y} | \tilde{W}, \tilde{x}^F, \tilde{\rho}^F, z^P, z^S) p(z^P, z^S | Y)}{q(z^P) q(z^S)} \right] \\ &\leq \log p(\tilde{Y} | Y). \end{aligned}$$

This is a standard definition of the ELBO, albeit for the posterior predictive distribution rather than the marginal likelihood (i.e. the prior predictive). By converting the log of a product of densities into a sum of log-density terms and noting that the expectations are over proposal distributions $p = p(\tilde{W}, \tilde{x}^F, \tilde{\rho}^F | z^P, z^S)$ and $q = q(z^P) q(z^S)$, we can write this ELBO as:

$$\begin{aligned} \text{ELBO}_{\tilde{Y}|Y} &= \mathbb{E}_{q,p} \left[\log p(\tilde{Y} | \tilde{W}, \tilde{x}^F, \tilde{\rho}^F, z^P, z^S) \right] - \\ &\quad \mathbb{E}_{q,p} \left[\log \frac{q(z^P) q(z^S)}{p(z^P, z^S | Y)} \right] \\ \text{ELBO}_{\tilde{Y}|Y} &= \mathbb{E}_{q,p} \left[\log p(\tilde{Y} | \tilde{W}, \tilde{x}^F, \tilde{\rho}^F, z^P, z^S) \right] - \\ &\quad \text{KL}(q(z^P) q(z^S) || p(z^P, z^S | Y)), \end{aligned}$$

From the standard decomposition of the ELBO we can also reason that,

$$\begin{aligned} \text{ELBO}_{\tilde{Y}|Y} &= \log p(\tilde{Y} | Y) - \\ &\quad \text{KL}(q(z^P) q(z^S) || p(z^P, z^S | \tilde{Y}, Y)), \end{aligned}$$

and therefore

$$\begin{aligned} \mathbb{E}_{q,p} \left[\log p(\tilde{Y} | \tilde{W}, \tilde{x}^F, \tilde{\rho}^F, z^P, z^S) \right] &= \\ &\quad - \text{KL}(q(z^P) q(z^S) || p(z^P, z^S | Y)) = \\ \log p(\tilde{Y} | Y) - \text{KL}(q(z^P) q(z^S) || p(z^P, z^S | \tilde{Y}, Y)), & \\ \mathbb{E}_{q,p} \left[\log p(\tilde{Y} | \tilde{W}, \tilde{x}^F, \tilde{\rho}^F, z^P, z^S) \right] = \log p(\tilde{Y} | Y) & \\ - \text{KL}(q(z^P) q(z^S) || p(z^P, z^S | \tilde{Y}, Y)) & \\ + \text{KL}(q(z^P) q(z^S) || p(z^P, z^S | Y)). & \end{aligned}$$

Since the variational distributions q were already optimized during training to minimize the KL divergence in the third term on the right hand side of the above equation, we can reason that it will be small compared to the KL divergence in the second term (between the variational distribution and the true posterior given the test data). The difference of KL's should therefore remain nonnegative, allowing us to use the expected log-likelihood as a lower bound to the log posterior predictive probability of the test data. Additionally, the low dimensionality ($D = 2$ in our experiments) of z^P and z^S compared to Y led the log likelihood to dominate the ELBO in all our experiments, a fact which should not be changed by passing to $\text{ELBO}_{\tilde{Y}|Y}$. This leads to Equation (12) in Section 5.

Neural Topographic Factor Analysis for fMRI Data

Table 4. Classification Details on ThreatVids dataset. “Voxel” indicates the ANOVA-SVM strategy on input data. NTFA performs consistently better than HTFA and closer to performing a completely supervised feature selection + classification pipeline on the input data.

| Subject | Voxel | | | NTFA | | | HTFA | | |
|---------|---------------|---------------|---------------|----------------------|----------------------|----------------------|----------------------|----------------------|----------------------|
| | Heights | Social | Spiders | Heights | Social | Spiders | Heights | Social | Spiders |
| 4 | .9018 ± .0263 | .9449 ± .0400 | .9583 ± .0589 | .8586 ± .0128 | .8914 ± .0893 | 1.000 ± .0000 | .8408 ± .0729 | .8958 ± .1031 | .8576 ± .0603 |
| 5 | .9062 ± .0765 | .9688 ± .0255 | 1.000 ± .0000 | .8497 ± .0331 | .9062 ± .1111 | .9653 ± .0260 | .5818 ± .1012 | .6176 ± .1696 | .7569 ± .1513 |
| 6 | .4182 ± .0841 | .2604 ± .0896 | .5417 ± .0780 | .4509 ± .1065 | .2679 ± .0631 | .6111 ± .0856 | .2976 ± .1443 | .3527 ± .1325 | .5799 ± .1464 |
| 7 | .4375 ± .0312 | .3750 ± .0625 | .3906 ± .0469 | .4375 ± .0000 | .4375 ± .0938 | .3594 ± .0000 | .5938 ± .0625 | .2500 ± .0000 | .2969 ± .1094 |
| 8 | .9896 ± .0147 | .8611 ± .1029 | 1.000 ± .0000 | .9568 ± .0138 | .9132 ± .0498 | .9896 ± .0147 | .7872 ± .1029 | .8021 ± .0390 | .9554 ± .0318 |
| 9 | .5565 ± .1741 | .4598 ± .0552 | .5729 ± .1538 | .5179 ± .1200 | .3586 ± .0638 | .4167 ± .1284 | .7381 ± .1034 | .7708 ± .1620 | .6389 ± .1029 |
| 10 | .9688 ± .0442 | .9583 ± .0295 | 1.000 ± .0000 | .9896 ± .0147 | .9479 ± .0531 | 1.000 ± .0000 | .9271 ± .0390 | .9375 ± .0442 | .9479 ± .0390 |
| 11 | .8601 ± .1297 | .9345 ± .0259 | .9375 ± .0675 | .8512 ± .1388 | .9003 ± .0331 | .8576 ± .0762 | .6622 ± .0406 | .8438 ± .0765 | .6910 ± .1756 |
| 12 | .3584 ± .1949 | .6667 ± .0642 | .6518 ± .1779 | .4896 ± .0820 | .5327 ± .1021 | .6146 ± .1699 | .3810 ± .2172 | .6057 ± .0807 | .5060 ± .1094 |
| 13 | .8795 ± .0907 | .9881 ± .0168 | .8472 ± .1094 | .9018 ± .0768 | .9777 ± .1021 | .8646 ± .1031 | .8036 ± .1536 | .8690 ± .0269 | .8611 ± .0322 |
| 14 | .8498 ± .0312 | .8906 ± .0469 | .9688 ± .0312 | .8125 ± .0000 | .8906 ± .0156 | 1.000 ± .0000 | .8750 ± .0312 | .9375 ± .0312 | .9844 ± .0146 |
| 15 | .8194 ± .0982 | .8750 ± .0884 | .9167 ± .0780 | .8368 ± .0682 | .9345 ± .0512 | .9473 ± .0737 | .6007 ± .1077 | .8557 ± .0807 | .8318 ± .1294 |
| 16 | .9618 ± .0344 | .9896 ± .0147 | .9464 ± .0126 | .9653 ± .0260 | .9896 ± .0147 | .9583 ± .0295 | .8472 ± .1094 | 1.000 ± .0000 | .9271 ± .0531 |
| 17 | 1.000 ± .0000 | .9226 ± .0552 | .8348 ± .0726 | .9062 ± .0442 | .8259 ± .0384 | .8780 ± .0400 | .9514 ± .0246 | .4688 ± .1169 | .8095 ± .1528 |
| 18 | .8125 ± .1421 | .6815 ± .1148 | .8065 ± .0845 | .6354 ± .1405 | .5848 ± .1678 | .5952 ± .0661 | .6840 ± .0723 | .5938 ± .0765 | .6964 ± .0526 |
| 19 | .8507 ± .0177 | .9435 ± .0439 | .8497 ± .0944 | .8785 ± .0299 | .9345 ± .0042 | .8363 ± .0773 | .8854 ± .0390 | .8140 ± .0432 | .6741 ± .1404 |
| 23 | .7031 ± .0469 | .8460 ± .0603 | .7240 ± .0677 | .8147 ± .0290 | .8147 ± .0290 | .8490 ± .0677 | .5848 ± .0223 | .6607 ± .0893 | .7552 ± .0885 |
| 25 | .8393 ± .0636 | .9514 ± .0354 | .9896 ± .0147 | .7604 ± .0390 | .9340 ± .0723 | .9896 ± .0147 | .6146 ± .1206 | .9410 ± .0214 | .9033 ± .0422 |
| 26 | .8438 ± .1562 | .5312 ± .0312 | .8237 ± .1049 | .6406 ± .1094 | .7604 ± .0521 | .8058 ± .0871 | .7701 ± .0513 | .5885 ± .0052 | .9531 ± .0469 |
| 28 | .7812 ± .0675 | .9658 ± .0292 | 1.000 ± .0000 | .9643 ± .0505 | .9673 ± .0021 | 1.000 ± .0000 | .8289 ± .1462 | .8690 ± .0517 | .9896 ± .0147 |
| 29 | .9524 ± .0673 | .9375 ± .0442 | 1.000 ± .0000 | .8720 ± .0864 | .9256 ± .0374 | .9271 ± .0531 | .9018 ± .0263 | .9464 ± .0126 | .9479 ± .0390 |

Table 5. Classification Details on Lepping dataset. “Voxel” indicates the ANOVA-SVM strategy on input data. NTFA performs consistently better than HTFA and closer to performing a completely supervised feature selection + classification pipeline on the input data.

| Subject | Voxel | | | | NTFA | | | | HTFA | | | |
|---------|-------------|-------------|-------------|-------------|--------------------|--------------------|--------------------|--------------------|--------------------|--------------------|--------------------|--------------------|
| | -Music | -Sounds | +Music | +Sounds | -Music | -Sounds | +Music | +Sounds | -Music | -Sounds | +Music | +Sounds |
| CTRL-1 | .750 ± .204 | .417 ± .429 | .583 ± .236 | .792 ± .118 | .750 ± .204 | .292 ± .212 | .958 ± .059 | .583 ± .312 | .958 ± .059 | .375 ± .270 | .917 ± .118 | .833 ± .236 |
| CTRL-2 | .625 ± .270 | .917 ± .118 | .917 ± .118 | .542 ± .059 | .792 ± .212 | 1.00 ± .000 | .792 ± .156 | .750 ± .204 | .667 ± .312 | .917 ± .118 | .708 ± .212 | .583 ± .236 |
| CTRL-3 | .125 ± .102 | .542 ± .295 | .708 ± .212 | .292 ± .212 | .583 ± .118 | .792 ± .295 | .875 ± .102 | .583 ± .118 | .708 ± .212 | .833 ± .118 | .792 ± .212 | .417 ± .118 |
| CTRL-4 | .792 ± .156 | .792 ± .156 | .667 ± .118 | .667 ± .118 | .917 ± .118 | .625 ± .102 | .750 ± .204 | .667 ± .118 | .875 ± .177 | .583 ± .118 | .833 ± .118 | .583 ± .118 |
| CTRL-5 | .708 ± .257 | .542 ± .328 | .833 ± .236 | .625 ± .102 | .667 ± .118 | .667 ± .312 | .875 ± .177 | .625 ± .177 | .750 ± .204 | .667 ± .236 | .833 ± .204 | .833 ± .118 |
| CTRL-6 | .500 ± .408 | .792 ± .156 | .667 ± .236 | .833 ± .236 | .417 ± .236 | .833 ± .118 | .917 ± .118 | 1.00 ± .000 | .583 ± .425 | .750 ± .204 | .958 ± .059 | 1.00 ± .000 |
| CTRL-7 | .792 ± .156 | .417 ± .425 | .583 ± .118 | .500 ± .204 | .917 ± .118 | .417 ± .425 | .333 ± .118 | .250 ± .204 | .833 ± .118 | .458 ± .412 | .500 ± .204 | .167 ± .236 |
| CTRL-8 | 1.00 ± .000 | .833 ± .118 | .861 ± .104 | .750 ± .204 | 1.00 ± .000 | .750 ± .000 | 1.00 ± .000 | .667 ± .118 | .917 ± .118 | 1.00 ± .000 | .917 ± .118 | .917 ± .118 |
| CTRL-9 | .583 ± .118 | .958 ± .059 | .708 ± .212 | .500 ± .000 | .417 ± .312 | .917 ± .118 | .917 ± .118 | .667 ± .118 | .750 ± .000 | .917 ± .118 | .875 ± .102 | .583 ± .236 |
| CTRL-10 | .625 ± .306 | .875 ± .102 | .375 ± .102 | .167 ± .118 | .375 ± .445 | .833 ± .118 | .250 ± .204 | .208 ± .156 | .917 ± .118 | .833 ± .118 | .750 ± .204 | 1.00 ± .000 |
| CTRL-11 | .458 ± .212 | .875 ± .177 | .542 ± .156 | 1.00 ± .000 | .333 ± .118 | 1.00 ± .000 | .333 ± .118 | 1.00 ± .000 | .583 ± .118 | .792 ± .156 | .500 ± .204 | 1.00 ± .000 |
| CTRL-12 | .833 ± .118 | .667 ± .236 | .875 ± .102 | .917 ± .118 | .750 ± .204 | .667 ± .312 | .833 ± .118 | .708 ± .059 | .750 ± .204 | .583 ± .118 | .792 ± .833 | .833 ± .236 |
| CTRL-13 | .708 ± .257 | .667 ± .312 | .917 ± .118 | .292 ± .257 | .917 ± .118 | .750 ± .354 | .750 ± .204 | .292 ± .257 | .667 ± .236 | .250 ± .204 | .708 ± .212 | .750 ± .204 |
| CTRL-14 | .583 ± .312 | .667 ± .312 | .333 ± .118 | .833 ± .118 | .625 ± .306 | .875 ± .102 | .333 ± .118 | .750 ± .204 | .667 ± .236 | .458 ± .156 | .417 ± .118 | .875 ± .177 |
| CTRL-15 | .625 ± .177 | .875 ± .177 | .583 ± .312 | .917 ± .118 | .583 ± .236 | .667 ± .471 | .500 ± .204 | .625 ± .102 | .583 ± .118 | .792 ± .295 | .083 ± .118 | .875 ± .177 |
| CTRL-16 | .875 ± .177 | .792 ± .212 | .458 ± .156 | .583 ± .312 | .917 ± .118 | .667 ± .118 | .333 ± .312 | .500 ± .204 | .875 ± .102 | .833 ± .118 | .500 ± .408 | .417 ± .236 |
| CTRL-17 | .668 ± .312 | .250 ± .204 | .792 ± .156 | .625 ± .102 | .375 ± .102 | .208 ± .212 | .833 ± .118 | .375 ± .270 | .708 ± .257 | .292 ± .257 | .792 ± .156 | .792 ± .212 |
| CTRL-18 | .708 ± .212 | .625 ± .368 | .833 ± .118 | .833 ± .118 | .833 ± .236 | .667 ± .118 | .917 ± .118 | .625 ± .177 | .917 ± .118 | 1.00 ± .000 | .917 ± .118 | .458 ± .328 |
| CTRL-19 | .875 ± .102 | 1.00 ± .000 | .542 ± .358 | .917 ± .118 | .958 ± .059 | .750 ± .204 | .500 ± .408 | .917 ± .118 | .833 ± .236 | .958 ± .059 | .333 ± .236 | .583 ± .236 |
| CTRL-20 | .833 ± .236 | .833 ± .118 | .542 ± .328 | .500 ± .000 | .792 ± .156 | .875 ± .102 | .417 ± .425 | .375 ± .102 | .583 ± .312 | .667 ± .118 | .458 ± .386 | .625 ± .306 |
| MDD-1 | .542 ± .358 | .750 ± .204 | .833 ± .118 | .083 ± .118 | .792 ± .156 | .750 ± .204 | .833 ± .118 | .167 ± .118 | .667 ± .118 | .667 ± .312 | 1.00 ± .000 | .167 ± .118 |
| MDD-2 | .667 ± .236 | .250 ± .000 | .833 ± .236 | .667 ± .312 | .667 ± .312 | .167 ± .118 | .750 ± .204 | .667 ± .312 | .667 ± .471 | .417 ± .236 | .792 ± .295 | .708 ± .059 |
| MDD-3 | .111 ± .157 | 1.00 ± .000 | .583 ± .312 | .250 ± .354 | .444 ± .342 | .889 ± .157 | .556 ± .416 | .250 ± .204 | .194 ± .142 | .889 ± .157 | .639 ± .307 | .000 ± .000 |
| MDD-4 | .792 ± .156 | .625 ± .102 | .750 ± .204 | .833 ± .118 | .833 ± .118 | .583 ± .312 | .750 ± .204 | .750 ± .000 | .708 ± .059 | .667 ± .236 | .542 ± .328 | .875 ± .102 |
| MDD-6 | .667 ± .312 | .583 ± .425 | .875 ± .102 | .917 ± .118 | .667 ± .312 | .750 ± .354 | .917 ± .118 | .625 ± .306 | .708 ± .212 | .625 ± .177 | .958 ± .059 | .792 ± .212 |
| MDD-7 | .542 ± .156 | .792 ± .156 | .417 ± .312 | .583 ± .312 | .542 ± .212 | .833 ± .118 | .750 ± .000 | .625 ± .102 | .625 ± .102 | .583 ± .118 | .708 ± .059 | .417 ± .312 |
| MDD-8 | .833 ± .118 | .583 ± .312 | .792 ± .212 | .417 ± .312 | .917 ± .118 | .417 ± .118 | .708 ± .328 | .333 ± .471 | .875 ± .102 | .542 ± .257 | .833 ± .118 | .333 ± .471 |
| MDD-9 | 1.00 ± .000 | .667 ± .118 | .875 ± .177 | .958 ± .059 | 1.00 ± .000 | .250 ± .204 | 1.00 ± .000 | .917 ± .118 | 1.00 ± .000 | .292 ± .328 | .750 ± .204 | .833 ± .118 |
| MDD-10 | 1.00 ± .000 | .875 ± .177 | .833 ± .236 | .583 ± .118 | 1.00 ± .000 | .917 ± .118 | .833 ± .236 | .500 ± .000 | .917 ± .118 | .375 ± .177 | .792 ± .212 | .708 ± .212 |
| MDD-11 | .625 ± .102 | .667 ± .118 | .792 ± .212 | .833 ± .118 | .542 ± .156 | .833 ± .118 | .875 ± .177 | .791 ± .156 | .458 ± .059 | .375 ± .306 | 1.00 ± .000 | .750 ± .204 |
| MDD-12 | .833 ± .236 | .417 ± .118 | .583 ± .118 | .792 ± .156 | .708 ± .328 | .333 ± .118 | .708 ± .212 | .583 ± .118 | .458 ± .156 | .167 ± .118 | .667 ± .118 | .375 ± .102 |
| MDD-13 | .667 ± .312 | .708 ± .257 | .250 ± .000 | .583 ± .118 | .917 ± .118 | 1.00 ± .000 | .417 ± .118 | .583 ± .118 | 1.00 ± .000 | .917 ± .118 | .583 ± .118 | .750 ± .204 |
| MDD-14 | .583 ± .236 | .833 ± .118 | .583 ± .312 | .583 ± .118 | .333 ± .118 | .792 ± .156 | .500 ± .204 | .667 ± .312 | .375 ± .102 | .625 ± .102 | .667 ± .118 | .583 ± .236 |
| MDD-15 | 1.00 ± .000 | .583 ± .236 | .750 ± .204 | .583 ± .118 | .833 ± .118 | .750 ± .204 | .833 ± .236 | .750 ± .204 | .583 ± .312 | .500 ± .408 | .792 ± .212 | .667 ± .118 |
| MDD-16 | .917 ± .118 | .458 ± .386 | .292 ± .257 | .375 ± .102 | .958 ± .059 | .458 ± .386 | .542 ± .386 | .542 ± .059 | .958 ± .059 | .625 ± .306 | .417 ± .236 | .375 ± .102 |
| MDD-17 | 1.00 ± .000 | .208 ± .059 | .667 ± .236 | .750 ± .204 | 1.00 ± .000 | .250 ± .204 | .500 ± .000 | .833 ± .118 | .875 ± .177 | .250 ± .000 | .792 ± .212 | 1.00 ± .000 |
| MDD-18 | .833 ± .236 | 1.00 ± .000 | .750 ± .000 | .917 ± .118 | .833 ± .236 | .333 ± .236 | .917 ± .118 | .917 ± .118 | .417 ± .118 | .292 ± .212 | .833 ± .118 | .583 ± .312 |
| MDD-19 | .750 ± .000 | .625 ± .177 | .583 ± .236 | .917 ± .118 | .750 ± .000 | .625 ± .102 | .750 ± .000 | .833 ± .118 | .917 ± .118 | .750 ± .204 | .583 ± .118 | .583 ± .236 |

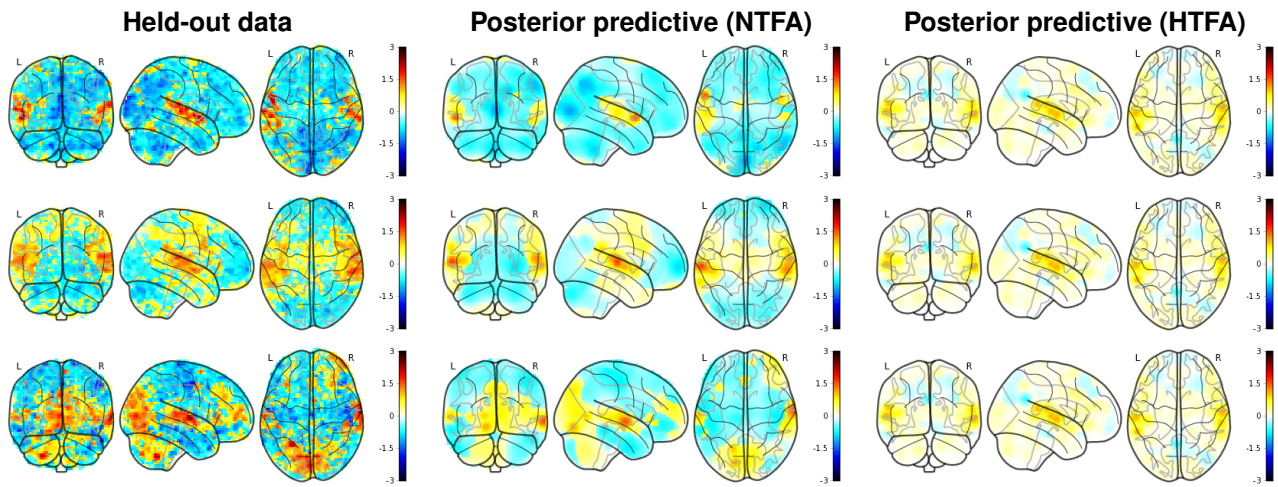


Figure 8. Test predictions for the Lepping dataset: We show average images for three trials, with participant-stimulus pairs held out from the training set. Posterior predictive estimates under NTFA (center) capture meaningful trial-specific variation in the original images (left), whereas HTFA can only re-use its same global template across differing trials (right).

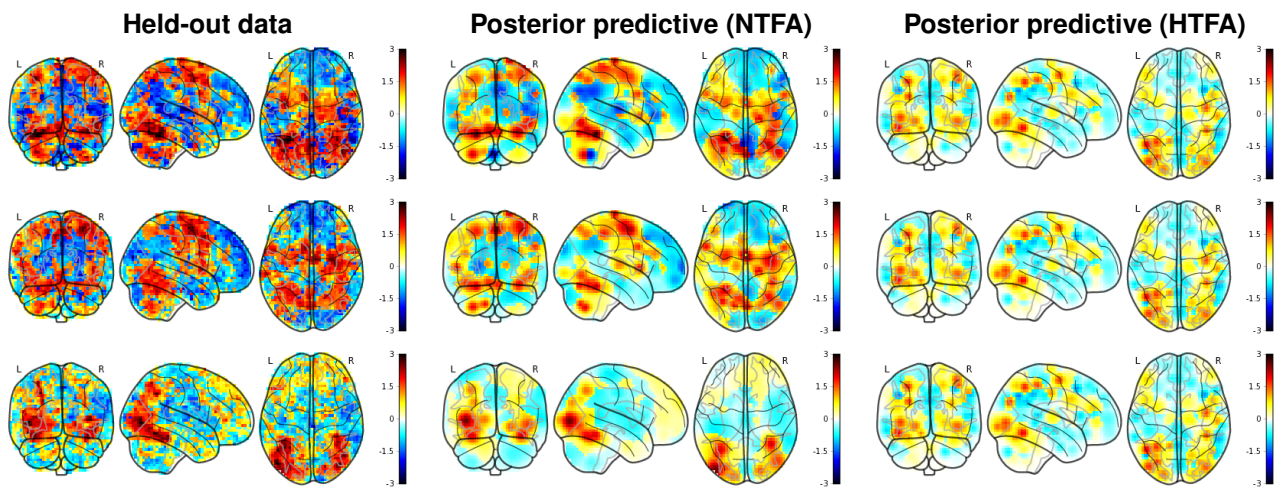


Figure 9. Test predictions for the Haxby dataset: We show average images for three trials, with participant-stimulus pairs held out from the training set. Posterior predictive estimates under NTFA (center) capture meaningful trial-specific variation in the original images (left), whereas HTFA can only re-use its same global template across differing trials (right).